Li *et al. Microstructures* **2025**, *5*, 2025019
DOI: 10.20517/microstructures.2024.11

Microstructures

Research Article

Open Access

The effect of dislocations on phase transition in $PbZrO_3$-based antiferroelectrics

Zhenqin Li[1,3], Zhengqian Fu[1], Tengfei Hu[1,4], Ziyi Yu[1,4], Linlin Zhang[1], Xuefeng Chen[2], Genshui Wang[1,2], Fangfang Xu[1,4]

[1]The State Key Laboratory of High Performance Ceramics and Superfine Microstructures, Shanghai Institute of Ceramics, Chinese Academy of Sciences, Shanghai 200050, China.
[2]The Key Lab of Inorganic Functional Materials and Devices, Shanghai Institute of Ceramics, Chinese Academy of Sciences, Shanghai 200050, China.
[3]Center of Materials Science and Optoelectronics Engineering, University of Chinese Academy of Sciences, Beijing 100049, China.
[4]School of Physical Science and Technology, ShanghaiTech University, Shanghai 201210, China.

Correspondence to: Prof. Zhengqian Fu, Prof. Fangfang Xu, The State Key Laboratory of High Performance Ceramics and Superfine Microstructures, Shanghai Institute of Ceramics, Chinese Academy of Sciences, 1295 Dingxi Road, Changning District, Shanghai 200050, China. E-mail: fmail600@mail.sic.ac.cn; ffxu@mail.sic.ac.cn

How to cite this article: Li, Z.; Fu, Z.; Hu, T.; Yu, Z.; Zhang, L.; Chen, X.; Wang, G.; Xu, F. The effect of dislocations on phase transition in $PbZrO_3$-based antiferroelectrics. *Microstructures* **2025**, *5*, 2025019. https://dx.doi.org/10.20517/microstructures.2024.11

Received: 1 Feb 2024 **First Decision:** 8 Apr 2024 **Revised:** 14 May 2024 **Accepted:** 23 May 2024 **Published:** 21 Feb 2025

Academic Editor: Zibin Chen **Copy Editor:** Ting-Ting Hu **Production Editor:** Ting-Ting Hu

Abstract

Dislocations in perovskite oxides have an important influence on their macroscopic performances. In this work, we report abundant dislocations in $PbZrO_3$-based antiferroelectric (AFE) ceramics, which manifest themselves mainly as dislocation arrays with Burgers vectors along the <110> direction. We demonstrate that these dislocation arrays were emitted from the grain boundaries and exhibit a pure screw character with glide systems of <110>$\{1\bar{1}0\}$. The *in situ* transmission electron microscopy investigations indicate that dislocations are beneficial for stabilizing the AFE phase in the heating process and serve as nucleation sites for the AFE phase during cooling. Meanwhile, the stress field of dislocation arrays also plays a critical role in the growth of AFE domains, which can be applied for regulating domain size and orientation. These findings provide the basis for dislocation engineering in AFE ceramics.

Keywords: $PbZrO_3$-based antiferroelectric ceramics, dislocations, temperature-induced phase transition, AFE domains

INTRODUCTION

Dislocations in perovskite oxides have always been one of the main topics of extended-defect research due to their wide influence on the overall performance. Prominent examples include acceleration of oxygen ion diffusion[1], variation of ionic transport performance[2,3], nucleation and pinning of domain walls[4-6], increased toughness[7], and influence on the local ferroelectric (FE) polarization[8]. Up to now, dislocation structures have been investigated in depth in perovskite oxides of $SrTiO_3$, $BaTiO_3$, $MgSiO_3$, etc. In particular, Höfling *et al.* found that introducing dislocation network with uniaxial compression could force $BaTiO_3$ single crystal to form a domain structure that consequently enhanced the piezoelectric coefficient by a factor of 19[9]. This indicates that dislocations could be a useful tool for optimizing properties of functional oxides. To date, the studies of dislocations in perovskite oxides covered quantum paraelectrics (PEs), FEs and linear dielectrics, but except for antiferroelectrics (AFEs) whose prototypical structure exhibits a specific polarization modulation derived from the cubic perovskite.

$PbZrO_3$-based AFEs are promising candidates for dielectric energy storage capacitors owing to the involvement of high energy and power density during the electric-induced AFE-FE phase transition[10-15]. The recoverable energy storage density of $PbZrO_3$-based capacitors reaches up to 10.4 J/cm^3[16], representing a significant advancement in capacitor technologies. However, being limited by a short lifetime, to date, AFE capacitors cannot fully utilize their excellent energy storage performance in practical applications. The large strain induced by the large volume change during polarization switching in AFE-FE phase transition usually leads to cracking or even failure of the AFE material, thereby reducing the lifetime of capacitors[17-20]. It is well known that dislocations are usually expected to engineer strain fields to tune mechanical properties of materials. However, how dislocations interact with phase transition or domain wall motion in AFE remains unclear. Thus, it is highly desired to investigate dislocations in AFE, which may promote strategies such as regulating domain size or dispersing phase transition to suppress sharp volume change for an enhanced lifetime.

Here, we mainly applied transmission electron microscopy (TEM) and investigated the effect of dislocations on phase transition in $(Pb_{0.97}La_{0.02})(Zr_{0.50}Sn_{0.50})O_3$ (PLZS) AFE ceramics. PLZS, an orthorhombic AFE phase at room temperature, transforms to the cubic PE phase at the Curie temperature of around 146 °C. It is found that the considerably high density of dislocations manifests themselves in arrays and has multiple influences on the stability of the AFE phase during temperature-induced phase transition, showing promising potential for dispersing the phase transition process, hence avoiding sharp volume changes and risk of material failure.

METHODS

Materials synthesis

PLZS ceramics were obtained using traditional high-temperature solid-phase sintering methods. The raw materials for sintering PLZS are Pb_3O_4, La_2O_3, ZrO_2 and SnO_2 powders with purity higher than 99.0%. Because Pb volatilizes during sintering, a small amount of excess PbO (0.5 wt%) was added. The preparation process of PLZS was as follows: firstly, the raw material powders were mixed and ball milled for 6 h, dried at 120 °C, and then calcined at 900 °C for 2 h. The obtained PLZS powders were ball milled again for 24 h, dried at 120 °C, mixed with 6 wt% PVA as a binder, and then pressed into disks with a diameter of 13 mm at 150 MPa. Lastly, the binder was burned out at 800 °C for 2 h, and the disks were sintered at 1,300 °C for 2 h.

Materials characterizations

The TEM specimens were prepared from ceramic bulk by mechanical thinning, polishing, and Ar^+ ion-milling in a gatan precision ion polishing System (PIPS) II, and finally, a thin carbon film was sprayed with

a thickness of 3 nm. In order to decrease ion-beam damage during ion-milling, the ion-beam voltage was gradually decreased from 3 to 0.5 keV. TEM investigation was performed on a JEM-2100F equipped with a heating holder (Gatan Model 652). *In situ* X-ray diffraction (XRD) experiment was conducted on a Rigaku D/max 2,550 V diffractometer using Cu-Kα radiation in the 2θ range of 10°-110° with a scanning speed of 10° per minute and a step of 0.2°. This temperature range measured in the *in situ* XRD experiment is 25 to 350 °C, with a rate of 10 °C per minute.

RESULTS AND DISCUSSION

Characterization of dislocations

Extensive TEM examinations indicate universal appearance of dislocations in PLZS AFE ceramics, as shown in Figure 1. Compared with those reported in other perovskite oxides, the most notable feature of dislocations in PLZS AFE ceramics is that they manifest themselves as dislocation arrays and networks, which mainly distribute within grains and always across the domain walls. Individual dislocations could also be observed, but in very small amounts. They usually project along the <110> and <001> directions (all crystallographic indices refer to the simple pseudocubic unit cell in this work), similar to those reported in $SrTiO_3$[21].

The Burgers vector b and line direction *l* are the main parameters for the characterization of dislocations. From the two parameters, the possible slip system of dislocations can be deduced. Figure 2 shows the characterization of Burgers vector b of dislocations, determined by invisibility criteria $g \cdot b = 0$. The condition $g \cdot b = 0$ signifies the reflection vector g is normal to b, and dislocations meeting this criterion are displayed out of contrast in the two- or weak-beam dark-field (DF) micrographs. Figure 2A and B was acquired using two reflection vectors $g = [10\bar{1}]$ and $g = [020]$, respectively, after large-angle tilting of the sample to near the [101] zone axis, while Figure 2C was attained using $g = [121]$ near the $[3\bar{2}1]$ zone axis. It can be seen that the contrast of the dislocation array in Figure 2B and C was weak, which is similar to the contrast of dislocations in alloys when $g \cdot b = 0$[22]. Their strong residual contrasts are due to the large magnitude of the Burgers vector and the strong free surface relaxation. That is to say, the dislocation array is out of contrast under reflection vectors $g = [020]$ and $g = [121]$, while it is visible under $g = [10\bar{1}]$. Thus, the Burgers vector of the present dislocation array could be determined as $[10\bar{1}]$, belonging to the <110>-type. In oxide perovskites, including $SrTiO_3$[23] and $BaTiO_3$[9], dislocations with Burgers vector of <110> have been widely reported.

The line direction *l* is determined by performing a trace analysis during tilting. The line contrast of dislocations indicates a projection of the dislocation lines along the [101] viewing direction [Figure 2D]. With the line projections parallel to $[10\bar{1}]$ [Figure 2E], the line direction *l* of dislocations could refer to $[10\bar{1}] \pm n[101]$, which means the possible direction includes $[10\bar{1}]$, [100] and [001]. As shown in Figure 2A-C and 2F, when this grain is rotated around the $g = [10\bar{1}]$ or $g = [010]$ in order to obtain a two-beam condition for DF imaging, the length of dislocations varies accordingly. Via tracing the dislocation length variation during tilting, it is found that the projected line length of dislocations in Figure 2A is similar to that in Figure 2E, while that in Figure 2B is significantly shortened. Therefore, we finally determine that the line direction ***l*** is along the $[10\bar{1}]$ direction.

Based on the above analyses, it can be inferred that these dislocation arrays have the glide system of the $<110>\{1\bar{1}0\}$, whose characteristic is pure screw. The Peierls-Nabarro model suggested that this is the easiest system for slipping in perovskite oxides[24]. In addition, the system is responsible for the plasticity in $SrTiO_3$ single crystals at room temperature[25]. Kondo *et al.* observed in real-time the formation of this system under the action of nanoindentation in $SrTiO_3$[23].

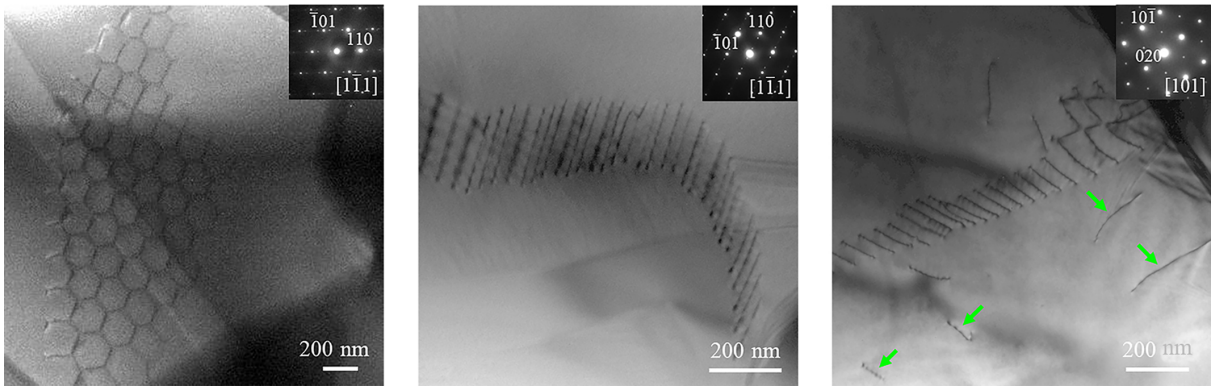

Figure 1. Dislocations in different grains of the present PLZS sample. The green arrows indicate the individual dislocations. PLZS: $(Pb_{0.97}La_{0.02})(Zr_{0.50}Sn_{0.50})O_3$.

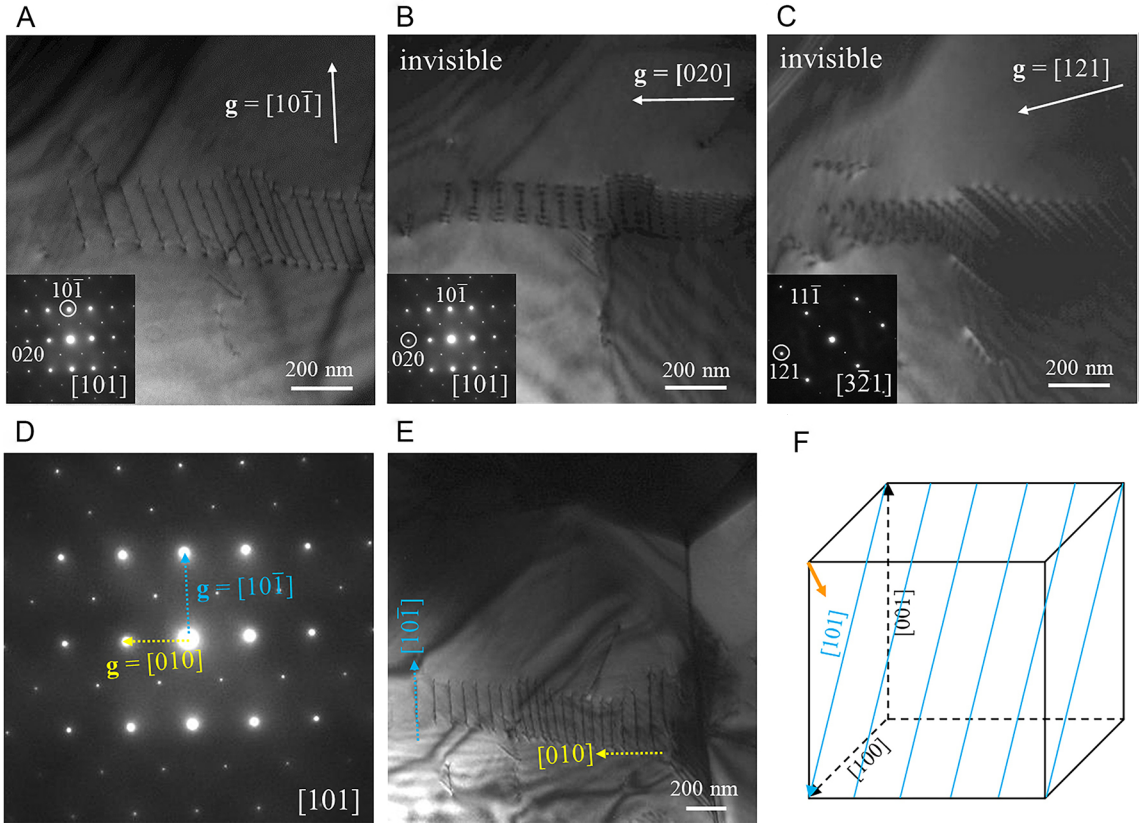

Figure 2. Characterization of dislocation arrays in PLZS. (A-C) The two-beam dark-field micrographs of the identical area using an operating vector of g = [10$\bar{1}$], [020] and [121], respectively; (D) the selected-area electron diffraction pattern; (E) the corresponding bright-field micrograph; (F) the schematic drawing of dislocation arrays. The blue and yellow arrows in (E) indicate the directions of dislocation lines and array layout, respectively. The orange arrow and blue lines in (F) denote the electron-beam direction and dislocations. PLZS: $(Pb_{0.97}La_{0.02})(Zr_{0.50}Sn_{0.50})O_3$.

Most dislocations in perovskite oxides, including $SrTiO_3$[21], $BaTiO_3$[9] and $KNbO_3$ single crystals[4], are activated by a compressive stress at high temperatures. For PLZS ceramics, the stress to activate the dislocations most likely comes from the strain generated during cooling in the synthesis. Figure 3A shows the *in situ* XRD examination upon decreasing the temperatures. At a high temperature of 350 °C, PLZS

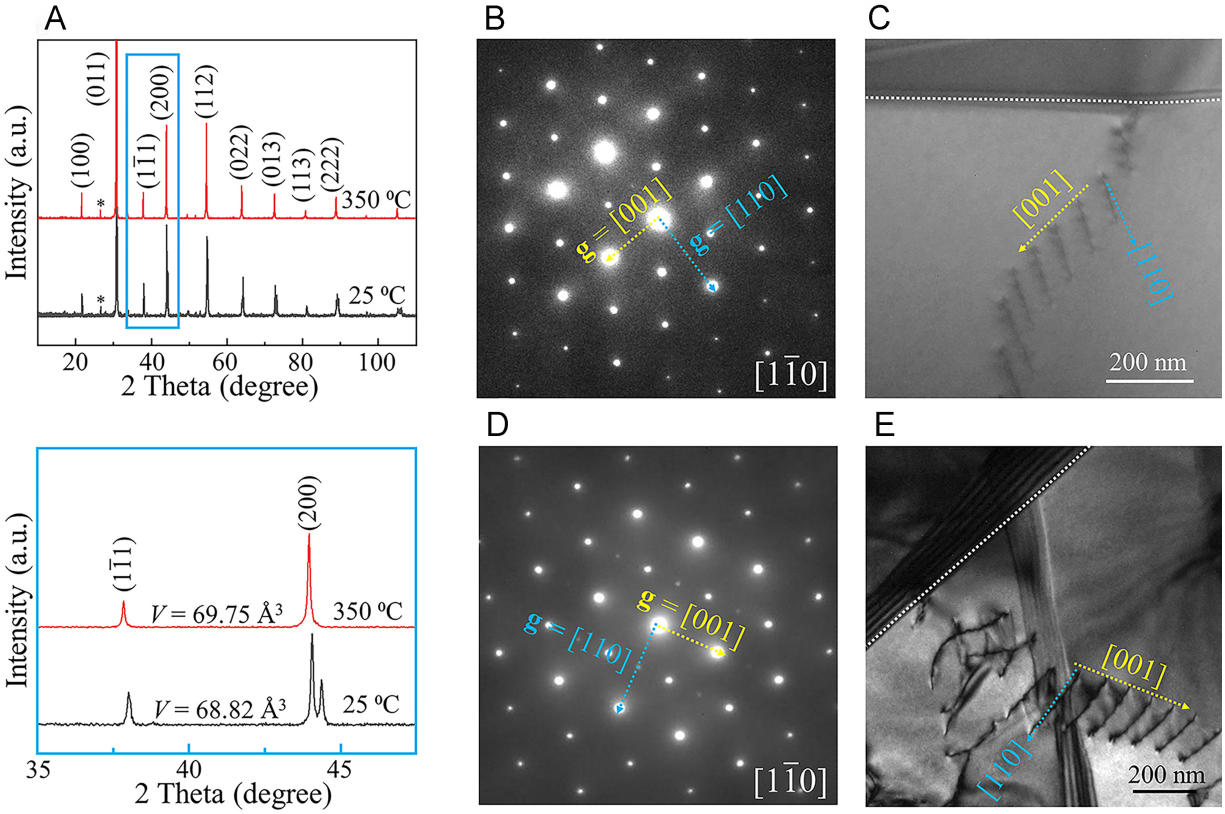

Figure 3. (A) XRD patterns of PLZS at 25 C and 350 C. At 350 C, the lattice parameters are $a = b = c = 4.1164$ Å, and the unit volume is $V = 69.75$ Å^3. At 25 C, the lattice parameters are $a = b = 4.113$ Å, $c = 4.085$ Å, and the unit volume is $V = 68.82$ Å^3. So, the volume shrinkage during cooling is $V = (V_{25\,°C} - V_{350\,°C}) / V_{350\,°C} = -1.33\%$; (B-E) nucleation of dislocation array at the grain boundaries in PLZS. The white dashed lines indicate the grain boundary. The blue and yellow arrows represent the directions of dislocation lines and array layout, respectively. PLZS: $(Pb_{0.97}La_{0.02})(Zr_{0.50}Sn_{0.50})O_3$.

exhibits a simple cubic perovskite structure of the PE phase, which is evidenced by non-split {*hoo*}, {*hho*} and {*hhh*} peaks. After cooling to room temperature, the PLZS spontaneously transits from the PE to AFE phase, accompanied by significant volume shrinkage up to -1.33%. Therefore, it is believed that large volume shrinkage arising from temperature-induced phase transition has induced considerable strains and provided enough driving force for forming dislocations in PLZS. A similar phenomenon has been widely reported in alloys[26,27].

Because the strain is usually concentrated at the bends or steps, grain boundaries should have accumulated the largest strain and consequently behave as nucleation sites for dislocations[28,29]. As seen in Figure 3B and C, Figure 3D and E dislocation arrays have indeed been emitted from the grain boundaries. This phenomenon makes sense because when a screw dislocation moves along the <001> direction, the required Peierls stress to overcome the energy barrier is minimal[24]. The gliding vectors of the dislocation arrays in Figure 2E and Figure 3C and E are along the [010] and [001] directions, respectively; the dislocation is emitted in the <001> direction, consistent with the moving direction of screw dislocations, as has been observed in the literature[23].

Effect of dislocations on the phase transition

In situ TEM via changing the temperatures has been employed to investigate the effect of dislocations on the phase transition. The selected zone axis for the present *in situ* TEM examination is along the [001] direction

at which the AFE and PE phases could be explicitly discriminated. The red framed region in Figure 4A (corresponding electron diffraction is shown in Figure 4B) was enlarged and monitored during the *in situ* heating [Figure 4C] and cooling [Figure 4D] processes. At 20 °C, satellite reflections in the fast Fourier transform (FFT) are both visible in areas 1 (near the dislocation) and 2 (away from the dislocation). Upon heating to 120 °C, the satellite reflections disappear in area 2 while they remain in area 1. The satellite reflections are associated with antiparallel alignment of A-site cations in the AFE phase[30], and its disappearance indicates that the AFE phase has transformed to the PE phase. Therefore, dislocations could stabilize the AFE phase during heating. Until the sample is heated to 160 °C, all satellite reflections disappear in area 1, suggesting full transition to the PE phase. Upon cooling from 160 °C and when the temperature reached 135 °C, interestingly, satellite reflections started to appear on the FFT of area 1 while they were still absent in area 2 [Figure 4D]. This suggests that the AFE phase preferentially nucleates near the dislocations during the PE-AFE phase transition. The present reversible *in situ* TEM investigation indicates that dislocations favor the stabilization of the AFE phase.

$PbZrO_3$-based AFEs demonstrate a distorted perovskite structure with antiparallel Pb-cation displacements. Such a structure is equivalent to a perovskite with modulated structure of $1/N$ {110}, i.e., a wavelength of N layers of its pseudocubic {110} plane[31-33], and N is termed as modulation period. It is similar to our previous discovery of the electric devil's staircase phenomenon[34], i.e., the modulation period shows a step-like change with temperature. In the present *in situ* study, the modulated structure of the AFE phase in PLZS again exhibits a stepwise variation during heating but shows difference between dislocation [Figure 4E] and non-dislocation areas [Figure 4F]. As shown in Figure 4B, the modulation period N of PLZS at room temperature could be obtained as four multiples by: $N = d_{110}/\lambda$. Multiple characterization methods, including XRD[35], electron diffraction[34-36] and aberration-corrected TEM[34,35], have confirmed this previously. Therefore, based on the shape and position of satellite reflections, it can be inferred that the modulation period referred to by the purple lines is around 4 [Figure 4E and F], by the orange lines is around 4.5, and by the red lines is around 5. It can be seen that a certain modulation period can be maintained within a comparatively wide temperature range. Moreover, the dislocations [Figure 4E] are found to further expand the temperature range of the stages, especially for stages 2 and 3. The ranges of stages 2 and 3 in area 2 (non-dislocation area) are 62-72 °C and 82-92 °C, respectively, while they expand to 62-82 °C and 92-120 °C, respectively, in area 1 (dislocation area) along with the duration of the AFE phase at higher temperatures. The AFE phase has transformed to the PE phase at 120 °C in the non-dislocation area [stage 4 in Figure 4F] while it remains available in the dislocation area [stage 3 in Figure 4E]. As a result, dislocations slow the transition rate among different modulated structures by extending the temperature range of stages in the electric devil's staircase, thus stabilizing the AFE phase during heating. Such discovery further indicates that the existence of dislocations disperses the phase transition of the whole system in a wider temperature range, potentially avoiding abrupt volume changes.

Compared to area 2, the lattice parameters in area 1 are significantly reduced [Table 1]. The previous atomistic simulation study on <110> screw dislocations in oxide perovskites considered that the dislocation causes distortion of the BO_6 octahedra and, especially, the AO_{12} cub-octahedra and, thus, generates local electric dipole moments inside the core[37]. Thereafter, we infer that the large electric dipole moments of A-site atoms around the dislocation core are responsible for stabilizing the AFE phase.

Besides stabilizing the AFE phase near dislocations, it is found that the dislocation array, in the meantime, plays a specific role in the evolution of AFE domains. Figure 5 demonstrates a large-field view of both domain and dislocation arrays subject to an *in situ* heating and cooling process in TEM. Here, the domain marked by yellow dash lines is pinned by a dislocation array, resulting in a controlled motion of domain

Table 1. The lattice parameters measured on FFT patterns at room temperature

	a (Å)	b (Å)
Area 1	4.174	4.161
Area 2	4.203	4.196

FFT: Fourier transform.

walls, hence regulating the domain size. As shown in Figure 5A-C and Supplementary Materials Video 1, upon increasing the temperature, the domain started to shrink from dislocation array β because of its wedge tip and eventually disappeared at the dislocation array α [see yellow-arrowed site in Figure 5C]. As shown in Figure 5D and E and Supplementary Materials Video 2, upon cooling, highlighted by yellow arrows in Figure 5E, domain walls nucleated at dislocation array α, then crossed the whole dislocation array α and terminated at dislocation array β. It seems that the dislocation array can provide a strong stress field nearby, which is evidenced by the following three phenomena during domain growth [Figure 5D-F]: (1) the width of domain is similar to that of the dislocation array α and was not further broadened; (2) the domain cannot grow as a lamellar shape but form wedged shape when it approaches close to the dislocation array β; (3) the domain wall can pass through the dislocation array α with a smaller crossing angle but terminate at one side of dislocation array β which is nearly perpendicular to the domain growth direction. These phenomena indicate that dislocation arrays can be critical in manipulating domain size and orientation.

According to the theoretical calculations in $KNbO_3$ FE perovskite oxide[4], the strong axial elastic field of linear screw dislocations[38,39] exerts a long-range influence on the polarization, which not only cause a rotation of the polarization vector around the dislocation line but also significantly increase the magnitude of polarization at the cores of dislocations. As a result, if a domain nucleates at the dislocation, the axial elastic field of the screw dislocation seems to preferentially promote its growth in a direction at a smaller angle to the direction of the dislocation array [see Figure 5E]. Nevertheless, the detailed reasons should be further investigated in the future.

CONCLUSIONS

In summary, this study elucidates the structure of dislocations in $PbZrO_3$-based AFEs and their roles in the temperature response to the modulated structures and formation of AFE domains. One of the most distinctive features in PLZS is the variety of dislocation arrays, which, however, have the identical glide system of $<110>\{1\bar{1}0\}$ with pure screw character, the easiest gliding system in perovskite oxides. The dislocation arrays are found not only to stabilize the AFE phase during phase transition but also to play critical roles in the growth of AFE domain walls. Thus, the present work provides a deep understanding of dislocations and their effects on the phase stabilization and domain morphologies in $PbZrO_3$-based AFEs, laying the foundation for subsequent property tailoring via dislocation engineering, such as modulating dislocation density by applying press in the synthesis or using flash sintering[40].

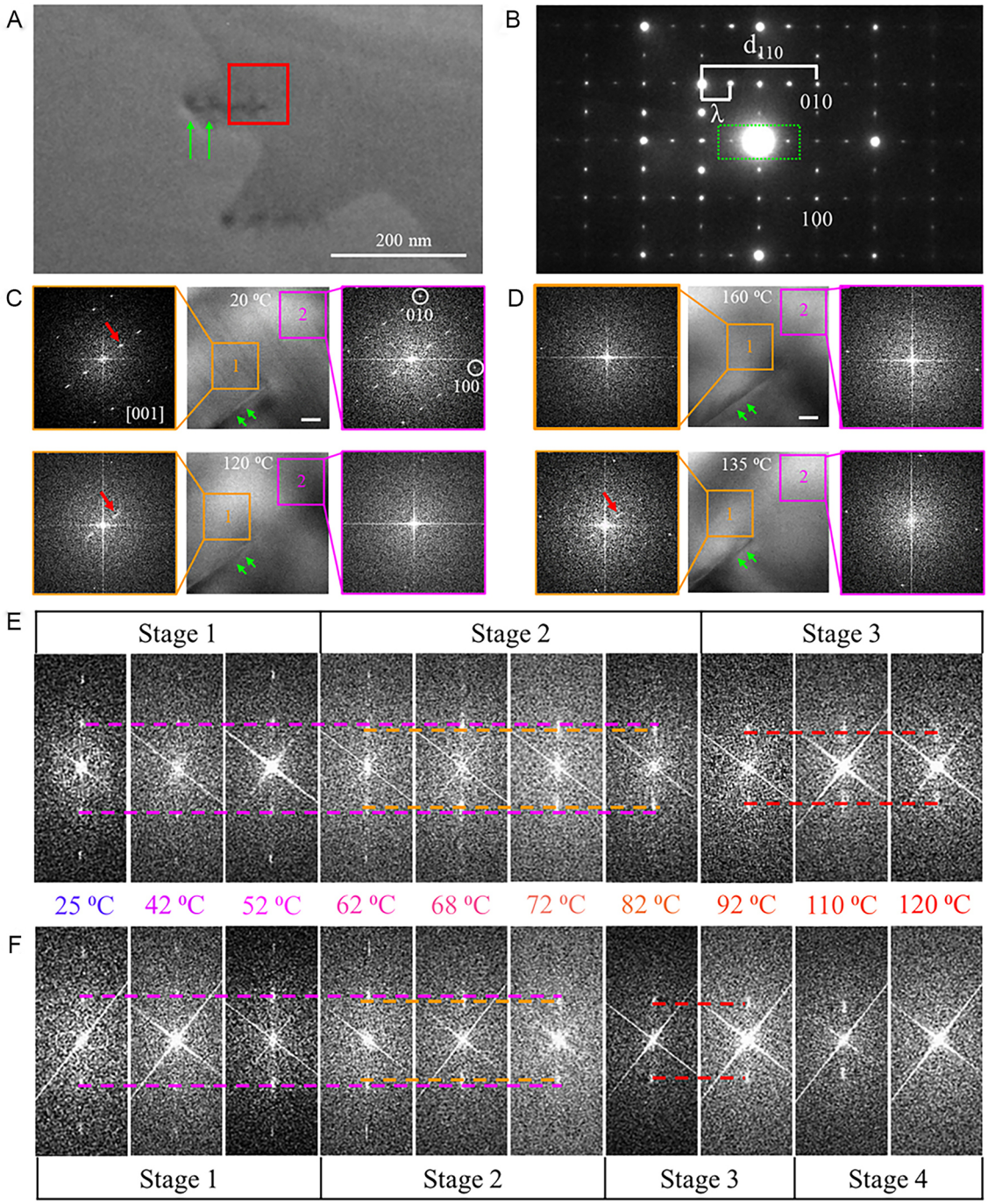

Figure 4. (A) The bright-field micrograph at room temperature showing a dislocation array near the domain boundary. The green arrows indicate the dislocations; (B) the [001] selected-area electron diffraction pattern obtained from framed area in (A), showing the modulated wave along the [110] direction. The modulation period *N* is counted by: $N = d_{110}/\lambda$, where d_{110} and λ are the distance measured in selected-area electron diffraction pattern; (C and D) present the *in situ* TEM of the green framed area in (A) during heating and cooling, respectively. The scale bar is 20 nm. Dislocations are indicated by green arrows. Areas 1 and 2 refer to dislocation and non-dislocation areas, respectively; (E and F) show the temperature dependence of FFT patterns in areas 1 and 2, respectively. TEM: Transmission electron microscopy; FFT: fourier transform.

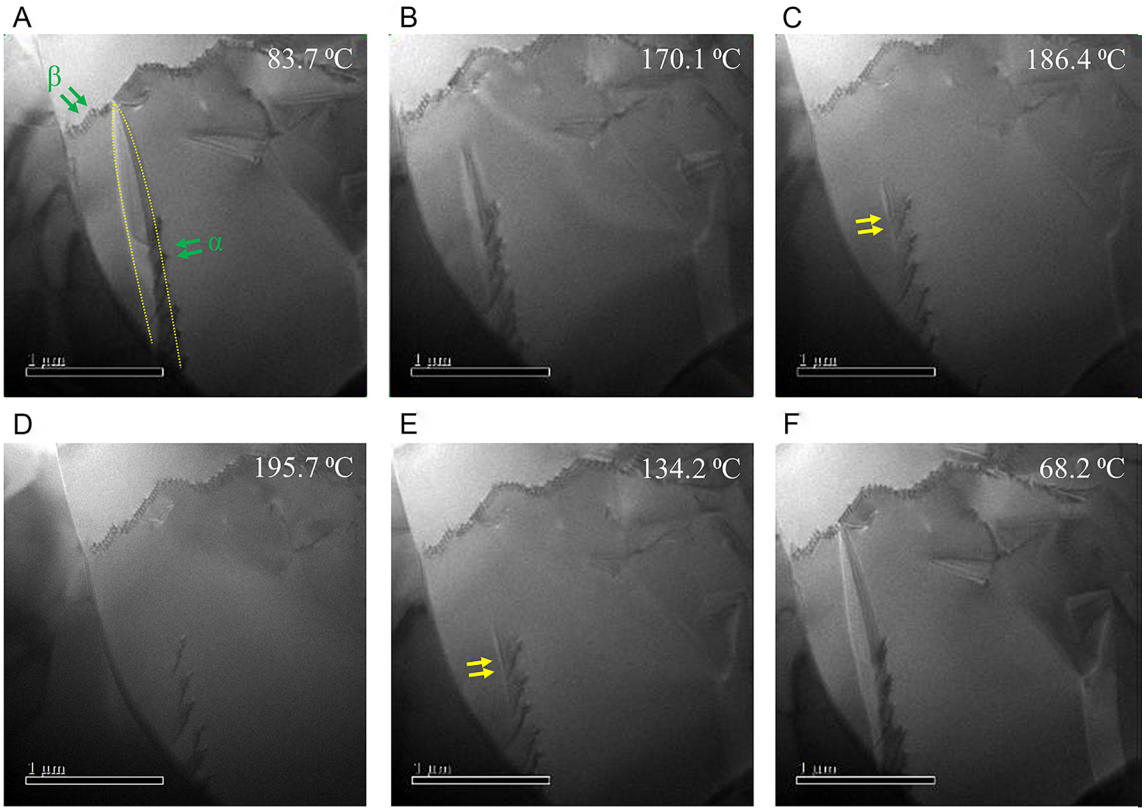

Figure 5. The bright-field observations of the evolution of AFE domains during (A-C) heating and (D-F) cooling in PLZS. The yellow dashed lines and arrows in (A, C, and E) indicate the AFE domain wall. The green arrows depict dislocation arrays. AFE: Antiferroelectric; PLZS: $(Pb_{0.97}La_{0.02})(Zr_{0.50}Sn_{0.50})O_3$.

DECLARATIONS

Authors' contributions

Made substantial contributions to the conception and design of the study and performed data analysis and interpretation: Liu, Z.; Fu, Z.; Xu, F.

Performed data acquisition and provided administrative, technical, and material support: Liu, Z.; Fu, Z.; Hu, T.; Yu, Z.; Zhang, L.; Chen, X.; Wang, G.; Xu, F.

Availability of data and materials

Not applicable.

Financial support and sponsorship

This work was supported by the National Natural Science Foundation of China (Grant No. 52002388); Young Elite Scientists Sponsorship Program by CAST (2022QNRC001); Shanghai Rising-Star Program (23QA1410800); Shanghai Science and Technology Innovation Action Plan (21ZR1472400), and Shanghai Technical Platform for Testing and Characterization on Inorganic Materials (19DZ2290700).

Conflicts of interest

All authors declared that there are no conflicts of interest.

Ethical approval and consent to participate

Not applicable.

Consent for publication

Not applicable.

Copyright

REFERENCES

1. Navickas, E.; Chen, Y.; Lu, Q.; et al. Dislocations accelerate oxygen ion diffusion in $La_{0.8}Sr_{0.2}MnO_3$ epitaxial thin films. *ACS. Nano.* **2017**, *11*, 11475. DOI PubMed PMC
2. De, S. R. A.; Fleig, J.; Maier, J.; et al. Electrical and structural characterization of a low-angle tilt grain boundary in iron-doped strontium titanate. *J. Am. Ceram. Soc.* **2003**, *86*, 922-8. DOI
3. Marrocchelli, D.; Sun, L.; Yildiz, B. Dislocations in $SrTiO_3$: easy to reduce but not so fast for oxygen transport. *J. Am. Chem. Soc.* **2015**, *137*, 4735-48. DOI PubMed
4. Hirel, P.; Mark, A. F.; Castillo-rodriguez, M.; Sigle, W.; Mrovec, M.; Elsässer, C. Theoretical and experimental study of the core structure and mobility of dislocations and their influence on the ferroelectric polarization in perovskite $KNbO_3$. *Phys. Rev. B.* **2015**, *92*, 214101. DOI
5. Gao, P.; Nelson, C. T.; Jokisaari, J. R.; et al. Revealing the role of defects in ferroelectric switching with atomic resolution. *Nat. Commun.* **2011**, *2*, 591. DOI PubMed
6. Xie, S.; Xu, Q.; Chen, Q.; Zhu, J.; Wang, Q. Realizing super-high piezoelectricity and excellent fatigue resistance in domain-engineered bismuth titanate ferroelectrics. *Adv. Funct. Mater.* **2024**, *34*, 2312645. DOI
7. Porz, L.; Klomp, A. J.; Fang, X.; et al. Dislocation-toughened ceramics. *Mater. Horiz.* **2021**, *8*, 1528-37. DOI PubMed
8. Jia, C. L.; Mi, S. B.; Urban, K.; Vrejoiu, I.; Alexe, M.; Hesse, D. Effect of a single dislocation in a heterostructure layer on the local polarization of a ferroelectric layer. *Phys. Rev. Lett.* **2009**, *102*, 117601. DOI PubMed
9. Höfling, M.; Zhou, X.; Riemer, L. M.; et al. Control of polarization in bulk ferroelectrics by mechanical dislocation imprint. *Science* **2021**, *372*, 961-4. DOI PubMed
10. Tan, X.; Ma, C.; Frederick, J.; Beckman, S.; Webber, K. G.; Green, D. J. The antiferroelectric↔ferroelectric phase transition in lead-containing and lead-free perovskite ceramics. *J. Am. Ceram. Soc.* **2011**, *94*, 4091-107. DOI
11. Hao, X.; Zhai, J.; Kong, L. B.; Xu, Z. A comprehensive review on the progress of lead zirconate-based antiferroelectric materials. *Prog. Mater. Sci.* **2014**, *63*, 1-57. DOI
12. Guo, B.; Jin, F.; Li, L.; Pan, Z.; Xu, X.; Wang, H. Design strategies of high-performance lead-free electroceramics for energy storage applications. *Rare. Met.* **2024**, *43*, 853-78. DOI
13. Cabral, M. J.; Chen, Z.; Liao, X. Scanning transmission electron microscopy for advanced characterization of ferroic materials. *Microstructures* **2023**, *3*, 2023040. DOI
14. Gao, B.; Qi, H.; Liu, H.; Chen, J. Role of polarization evolution in the hysteresis effect of Pb-based antiferroelecrtics. *Chin. Chem. Lett.* **2024**, *35*, 108598. DOI
15. Liu, H.; Zhou, Z.; Qiu, Y.; et al. An intriguing intermediate state as a bridge between antiferroelectric and ferroelectric perovskites. *Mater. Horiz.* **2020**, *7*, 1912-8. DOI
16. Wang, H.; Liu, Y.; Yang, T.; Zhang, S. Ultrahigh energy-storage density in antiferroelectric ceramics with field-induced multiphase transitions. *Adv. Funct. Mater.* **2019**, *29*, 1807321. DOI
17. Berlincourt, D.; Krueger, H.; Jaffe, B. Stability of phases in modified lead zirconate with variation in pressure, electric field, temperature and composition. *J. Phys. Chem. Solids.* **1964**, *25*, 659-74. DOI
18. Berlincourt, D. Transducers using forced transitions between ferroelectric and antiferroelectric states. *IEEE. Trans. Son. Ultrason.* **1966**, *13*, 116-24. DOI
19. Viehland, D.; Forst, D.; Xu, Z.; Li, J. Incommensurately modulated polar structures in antiferroelectric sn-modified lead zirconate titanate: the modulated structure and its influences on electrically induced polarizations and strains. *J. Am. Ceram. Soc.* **1995**, *78*, 2101-12. DOI
20. Hoover, B. D.; Tuttle, B. A.; Olson, W. R.; Goy, D. M.; Brooks, R. A.; King, C. F. Evaluation of field enforced antiferroelectric to ferroelectric phase transition dielectrics and relaxor ferroelectrics for pulse discharge capacitors. *Technical. Reports.* 1997. DOI
21. Taeri, S.; Brunner, D.; Sigle, W.; Rühle, M. Deformation behaviour of strontium titanate between room temperature and 1800 K under ambient pressure. *Int. J. Mater. Res.* **2022**, *95*, 433-46. DOI
22. Bonnet, R.; Loubradou, M. Crystalline defects in a B.C.T. Al2Cu(θ) single crystal obtained by unidirectional solidification along [001]. *phys. stat. sol. (a).* **2002**, *194*, 173-91. DOI
23. Kondo, S.; Mitsuma, T.; Shibata, N.; Ikuhara, Y. Direct observation of individual dislocation interaction processes with grain boundaries. *Sci. Adv.* **2016**, *2*, e1501926. DOI PubMed PMC

24. Ferré, D.; Carrez, P.; Cordier, P. Modeling dislocation cores in $SrTiO_3$ using the Peierls-Nabarro model. *Phys. Rev. B.* **2008**, *77*, 014106. DOI
25. Gumbsch, P.; Taeri-Baghbadrani, S.; Brunner, D.; Sigle, W.; Rühle, M. Plasticity and an inverse brittle-to-ductile transition in strontium titanate. *Phys. Rev. Lett.* **2001**, *87*, 085505. DOI PubMed
26. Li, J.; Zhou, J.; Xu, S.; et al. Effects of cryogenic treatment on mechanical properties and micro-structures of IN718 super-alloy. *Mater. Sci. Eng. A.* **2017**, *707*, 612-9. DOI
27. Wang, H.; Li, K.; Li, G.; et al. Microstructure and properties of spinning deformed A356 alloy subject to the solution-DCT-aging multiplex heat treatment. *J. Mater. Res. Technol.* **2023**, *23*, 5520-33. DOI
28. Murr, L. E. Some observations of grain boundary ledges and ledges as dislocation sources in metals and alloys. *Metall. Trans. A.* **1975**, *6*, BF02658408. DOI
29. Kacher, J.; Robertson, I. Quasi-four-dimensional analysis of dislocation interactions with grain boundaries in 304 stainless steel. *Acta. Mater.* **2012**, *60*, 6657-72. DOI
30. Asada, T.; Koyama, Y. La-induced conversion between the ferroelectric and antiferroelectric incommensurate phases in $Pb_{1-x}La_x(Zr_{1-y}Ti_y)O_3$. *Phys. Rev. B.* **2004**, *69*, 104108. DOI
31. Sawaguchi, E.; Maniwa, H.; Hoshino, S. Antiferroelectric structure of lead zirconate. *Phys. Rev.* **1951**, *83*, 1078. DOI
32. Ma, T.; Fan, Z.; Xu, B.; et al. Uncompensated polarization in incommensurate modulations of perovskite antiferroelectrics. *Phys. Rev. Lett.* **2019**, *123*, 217602. DOI PubMed
33. Gao, B.; Liu, H.; Zhou, Z.; et al. An intriguing canting dipole configuration and its evolution under an electric field in La-doped $Pb(Zr,Sn,Ti)O_3$ perovskites. *Microstructures* **2022**, *2*, 2022010. DOI
34. Li, Z.; Fu, Z.; Cai, H.; et al. Discovery of electric devil's staircase in perovskite antiferroelectric. *Sci. Adv.* **2022**, *8*, eabl9088. DOI PubMed PMC
35. Fu, Z.; Chen, X.; Li, Z.; et al. Unveiling the ferrielectric nature of $PbZrO_3$-based antiferroelectric materials. *Nat. Commun.* **2020**, *11*, 3809. DOI PubMed PMC
36. Hu, T.; Fu, Z.; Li, Z.; et al. Decoding the double/multiple hysteresis loops in antiferroelectric materials. *ACS. Appl. Mater. Interfaces.* **2021**, *13*, 60241-9. DOI PubMed
37. Hirel, P.; Mrovec, M.; Elsässer, C. Atomistic simulation study of <110> dislocations in strontium titanate. *Acta. Mater.* **2012**, *60*, 329-38. DOI
38. Hirth, J. P.; Lothe, J.; Mura, T. Theory of dislocations (2nd ed.). *J. Appl. Mech.* **1983**, *50*, 476-7. DOI
39. Bierman, M. J.; Lau, Y. K.; Kvit, A. V.; Schmitt, A. L.; Jin, S. Dislocation-driven nanowire growth and eshelby twist. *Science* **2008**, *320*, 1060-3. DOI PubMed
40. Cho, J.; Li, Q.; Wang, H.; et al. High temperature deformability of ductile flash-sintered ceramics via in situ compression. *Nat. Commun.* **2018**, *9*, 2063. DOI PubMed PMC